PAPER

Check for updates

Application of multilayer drug-loaded hydrogels in protection of open abdomen wounds

Runnan Wang, [ID] †[a] Kang Chen,†[b] Yilong Yu,†[cd] Guiwen Qu,[e] Qining He,[d] Helei Lu,[d] Rui Wang, [ID] [f] Yun Zhao,*[a] Jinjian Huang*[b] and Tao Zheng*[cd]

Open abdomen (OA) therapy is crucial for managing severe abdominal infections, intra-abdominal hypertension, and trauma but often faces complications like infections and enteric fistulas. To address this, a novel multilayer drug-loaded hydrogel dressing was designed to promote wound healing. The dressing comprises a bottom layer of a carboxymethyl chitosan/aldehyde-modified hyaluronic acid (CC/HA-CHO) hydrogel loaded with Ag nanoparticles (AgNPs) for rapid gelation and broad-spectrum antibacterial action; a middle polyacrylamide (PAAm) gel layer loaded with interleukin-4 (IL-4) to polarize macrophages toward the M2 phenotype for tissue repair; and a top polydimethylsiloxane (PDMS) antifouling layer treated with oxygen plasma for enhanced adhesion and hydrophilicity. Characterization *via* FTIR, SEM, swelling tests, and drug release assays confirmed the hydrogel's structure, stability, and sequential release of AgNPs and IL-4. *In vivo* experimental results show that the percentage of wound closure in the drug-loaded hydrogel group reached approximately 30% on day 7, while that in the control group was only about 10%. Thus, the drug-loaded hydrogel can significantly accelerate wound healing of open abdominal wounds. This multifunctional hydrogel combines antibacterial, anti-inflammatory, and tissue-regenerative properties, offering a promising strategy for OA wound management.

1. Introduction

Open abdomen (OA) therapy refers to the method of actively opening the abdominal cavity or leaving the abdominal incision unclosed after surgery, with temporary abdominal closure materials applied postoperatively to manage the wound. OA therapy helps reduce intra-abdominal pressure, control intra-abdominal infection, and promptly manage visceral organ injuries. It has become an essential therapeutic approach for severe abdominal trauma, severe intra-abdominal infections, and abdominal hypertension.[1–3] Despite its significant treatment effectiveness, early-stage OA therapy often leads to complications such as infection and enteroatmospheric fistulas

due to exposure of visceral organs, particularly the intestines. Therefore, to prevent enteroatmospheric fistulas, reduce bleeding, and prevent wound infection, temporary abdominal closure materials are commonly used in clinical practice.[1]

Traditional wound protection materials for the open abdomen include gauze packing, polypropylene mesh, decellularized matrix, and fibrin glue, which have limitations such as poor infection control, susceptibility to wound contamination, and potential intestinal erosion and necrosis.[4–6] An ideal wound dressing should possess: (1) excellent tissue compatibility without toxicity; (2) good moisture retention to maintain a moist wound environment and absorb wound exudate; (3) sufficient physical and mechanical strength to ensure dressing integrity and prevent bacterial invasion due to material breakage; (4) appropriate surface microstructure and biochemical characteristics to promote cell adhesion, proliferation, and differentiation.[7] Hydrogels, due to their excellent permeability, unique three-dimensional structure, and superior drug-loading capacity, are considered ideal biomaterials and have been extensively researched in recent years.[8]

Previous studies have shown that sandwich-structured hydrogels can achieve sequential release of multiple drugs through "time-spaced" delivery, demonstrating excellent therapeutic effects in infected wounds[9] (Table S1). Therefore, we designed a multilayer drug-loaded hydrogel dressing to promote healing of open abdomen wounds. From bottom to

[a]Department of Surgical Research Laboratory, BenQ Medical Center, The Affiliated BenQ Hospital of Nanjing Medical University, The Clinical Translational Research Center for Surgical Infection and Immunity of Nanjing Medical University, Nanjing, China. E-mail: zhaoyun@njmu.edu.cn

[b]Research Institute of General Surgery, Jinling Clinical Medical College, Nanjing Medical University, Nanjing, China. E-mail: jinjian_huang@seu.edu.cn

[c]Department of General Surgery, BenQ Medical Center, The Affiliated BenQ Hospital of Nanjing Medical University, Nanjing, China. E-mail: jefferyzheng@yeah.net

[d]Department of Abdominal Acute Care Surgery, General Surgery Center, Shanghai General Hospital, Shanghai Jiao Tong University School of Medicine, Shanghai, China

[e]School of Medicine, Southeast University, Nanjing, China

[f]State Key Laboratory of Materials-Oriented Chemical Engineering, Nanjing Tech University, Nanjing, China

† Runnan Wang, Kang Chen and Yilong Yu contributed equally to this work.

top, it consists of carboxymethyl chitosan (CC)/aldehyde hyaluronic acid (HA-CHO) hydrogel, polyacrylamide (PAAm) gel, and polydimethylsiloxane (PDMS) anti-fouling layer.[10–12]

CC, an important derivative of chitosan, exhibits high solubility and is often combined with other polymers to produce hydrogels with good biocompatibility and moisture-retaining properties.[13] HA is a major component of the extracellular matrix (ECM) and exhibits biodegradability, biocompatibility, non-toxicity, and viscoelasticity.[14] It promotes wound healing by enhancing granulation tissue formation, re-epithelialization, and angiogenesis through the stimulation of fibroblast proliferation and angiogenesis.[15] However, HA degrades easily under external tension, which may allow external bacteria to invade and cause wound infection. Studies have shown that aldehyde-modified HA can improve the self-healing ability of hydrogels.[15] Previous literature has reported that hydrogels formed by crosslinking CC with HA-CHO exhibit rapid gelation, good self-healing properties, and high drug loading capacity.[16,17] PDMS has excellent antifouling properties[10] and covering the hydrogel surface with it can prevent microorganisms from the external environment from contaminating the wound and the hydrogel. It has been documented that the synthesis of PAAm gel on the plasma-treated PDMS surface is feasible.[18]

Additionally, we loaded different functional drugs in the base and intermediate layers according to wound healing characteristics to precisely regulate wound healing. Silver nanoparticles (AgNPs) possess broad-spectrum and highly effective antibacterial activity, capable of effectively killing various pathogens such as *Escherichia coli*, *Klebsiella pneumoniae*, and *Staphylococcus aureus* even at very low concentrations.[19] Macrophages play a crucial protective role in wound cell proliferation and tissue recovery.[20] Increasing evidence suggests that macrophages play critical roles in every stage of normal healing, and disruption of their function may lead to prolonged inflammation and pathological healing.[21] Specifically, under infection conditions, macrophages polarize to the M1 type, secreting pro-inflammatory factors to combat bacterial infections;[22] during the tissue repair phase, macrophages polarize to the M2 type, secreting anti-inflammatory factors, transforming growth factor-beta (TGF-β), and chemokines to promote wound healing.[23] Research indicates that IL-4 can stimulate macrophage polarization towards the M2 type.[24] The functional differences of macrophages in infected wounds highlight the need for different drugs at various stages of wound healing to achieve effective wound healing. We loaded AgNPs in the base layer hydrogel for early-stage wound healing to exert antibacterial effects; IL-4 active protein was loaded in the intermediate layer to stimulate macrophage polarization towards the M2 type during tissue repair, thereby promoting wound healing (Fig. 1).

2.   Materials and methods

2.1   Materials

Sodium hyaluronate (HA, M_w: 150–250 kDa, Shanghai YUANYE Bio-Technology Co., Ltd), sodium periodate (ACS reagent ≥99.8%, Sigma-Aldrich, USA), ethylene glycol (Anhydrous ≥99.8%, Sigma-Aldrich, USA), carboxymethyl chitosan (CC,

degree of carboxylation ≥80%, Mw: 20 kDa Shanghai YUANYE Bio-Technology Co., Ltd), silver nanoparticle dispersion (AgNPs, Aladdin), acrylamide (AAm, Sigma-Aldrich, USA), N,N'-methylenebisacrylamide (MBAA, Aladdin), 2-hydroxy-4'-(2-hydroxyethoxy)-2-methylpropiophenone (Irgacure 2959, Aladdin), interleukin-4 (IL-4) active protein (Beijing Yun Clone Biotechnology Co., Ltd), polydimethylsiloxane (PDMS, Sylgard184, Dow Corning, USA), polytetrafluoroethylene mold (2.5 cm × 5 cm × 1 cm).

2.2   Synthesis of drug-loaded hydrogel dressings

2.2.1   Synthesis of CC/HA-CHO hydrogel loaded with AgNPs. Synthesis of HA-CHO: firstly, dissolve 1 g HA in 100 mL of distilled water to prepare a 1wt% solution. Add 5 mL of 0.5 mol per L sodium periodate solution and stir evenly. Allow the reaction to proceed in darkness at room temperature for 2 hours. Then, add 1 mL of ethylene glycol solution to terminate the reaction for 1 hour, neutralizing any unreacted sodium periodate. Transfer the reaction mixture into a dialysis membrane, change the dialysis solution every 8 hours for 3 days. Freeze-dry the dialyzed solution for 24 hours to obtain solid aldehyde-modified hyaluronic acid (HA-CHO). Dissolve the freeze-dried HA-CHO in distilled water to prepare a 60 mg per mL HA-CHO solution.[9]

Synthesis of CC: dissolve CC powder in distilled water to prepare a 24 mg per mL CC solution. Mix the 60 mg per mL HA-CHO solution and the 24 mg per mL CC solution in equal volumes. The cross-linking reaction between amino and aldehyde groups forms the CC/HA-CHO hydrogel.[25] To prepare CC/HA-CHO hydrogel loaded with AgNPs, pre-mix a dispersion of 40 μg per mL AgNPs in the HA-CHO solution.

2.2.2   Synthesis of PAAm hydrogel loaded with IL-4 active protein. The synthesis of PAAm hydrogel follows the method by Nakajima *et al.* Dissolve 2 g of AAm, 4 mg of cross-linker MBAA, and 50 mg of photoinitiator Irgacure 2959 in 10 mL of distilled water. Mix thoroughly and irradiate under a 365 nm UV lamp for approximately 1 minute to form the PAAm hydrogel.[26] Pre-mix a solution of 10 ng per mL IL-4 active protein in the precursor solution of PAAm to obtain IL-4 loaded PAAm hydrogel.

2.2.3   Preparation of PDMS anti-fouling coating. Following the method of Tian *et al.*, prepare the PDMS anti-fouling coating and treat the PDMS-hydrogel interface with oxygen plasma to improve hydrophilicity and adhesion.[12] Specific steps include mixing the main agent and curing agent of Sylgard184 at a ratio of 10 : 1, pouring into a polytetrafluoroethylene mold (2.5 cm × 5 cm × 1 cm), and heating at 65 °C for 1 hour. Due to its hydrophobic nature and weak adhesion, modify PDMS surface through plasma treatment. Place the cured PDMS into a vacuum plasma treatment device (PR80L) for surface treatment for 300 seconds (power: 300 w, gas: 150 sccm nitrogen + 50 sccm oxygen, vacuum degree: 30 PA). Exposure of PDMS to vacuum plasma converts surface methyl ($-CH_3$) groups to hydroxyl ($-Si-OH$) groups, enhancing surface hydrophilicity and facilitating grafting or polymerization with other materials.[27]

2.2.4   Assembly of drug-loaded hydrogel dressings. Firstly, synthesize PDMS anti-fouling layer in a polytetrafluoroethylene
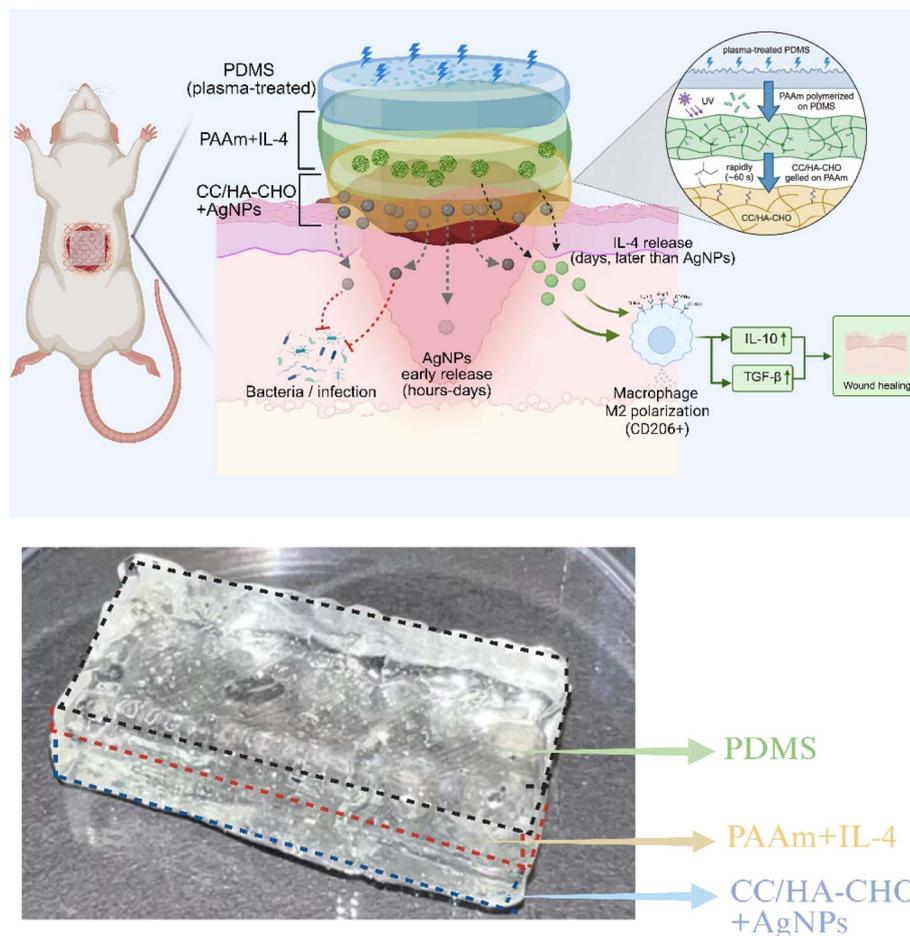
Fig. 1 Schematic illustration of the multilayer drug-loaded hydrogel synthesis process and the resulting product images.

mold (2.5 cm × 5 cm × 1 cm) and treat with plasma. Due to rapid recovery of hydrophobicity after treatment,[27] quickly synthesize IL-4 loaded PAAm on the surface of PDMS. Finally, pour AgNPs loaded CC/HA-CHO onto the surface of PAAm. After complete gelation of CC/HA-CHO (approximately 60 seconds), extrude the composite hydrogel from the mold. The multilayer drug-loaded hydrogel was used and stored as the final product in its hydrated hydrogel state (stored short-term in PBS solution at 4 °C) without undergoing final drying or freeze-drying.

2.3 Characterization of hydrogel dressings

2.3.1 PDMS surface properties testing. PDMS was overlaid with hydrogel to form a contact area of 0.5 cm × 0.5 cm. Using a universal mechanical tester equipped with a 1 kN load cell (Wance ETM103A, Shenzhen, China), the hydrogel was subjected to tensile testing at a rate of 5 mm min^{-1} to measure the adhesive strength of PDMS before and after plasma treatment. Each hydrogel sample underwent at least 5 repeated mechanical experiments. The adhesive strength of PDMS (kPa) was calculated using the formula $P = \frac{F}{S}$. Additionally, contact angle measurements were performed on PDMS before and after plasma treatment to confirm changes in hydrophilicity.

2.3.2 Contact angle measurement. Measurements were conducted using a commercial contact angle measurement system (First Ten Angstroms, FTA135) to assist with image capture. For each measurement, a single 10 μL droplet of deionized water was deposited on a previously untested area of the sample surface, followed by a 20-second delay to allow the wetting to stabilize before measurement. The experiment included an untreated group and an oxygen plasma-treated group. All samples were stored under a relative humidity of 47%. At least five measurements were performed for each group, and all measurements within the same group were completed within a five-minute period.[12] Contact angles are reported as mean ± SD.

2.3.3 Fourier transform infrared spectroscopy (FTIR) analysis of hydrogel. Firstly, freeze-dry PAAm hydrogel, CC/HA-CHO hydrogel, and HA-CHO for 24 hours. Grind the freeze-dried materials into powder and place them on dried KBr discs. Analyze using a spectrometer (Nicolet-6700, Thermo®, USA) in the range of 4000–500 cm^{-1} with a resolution of 4 cm^{-1}, alongside AAm, MBAA, CC, and HA powder.

2.3.4 Swelling behavior of CC/HA-CHO hydrogel and PAAm hydrogel. The swelling ratio of freeze-dried CC/HA-CHO hydrogel and PAAm hydrogel was measured using gravimetric
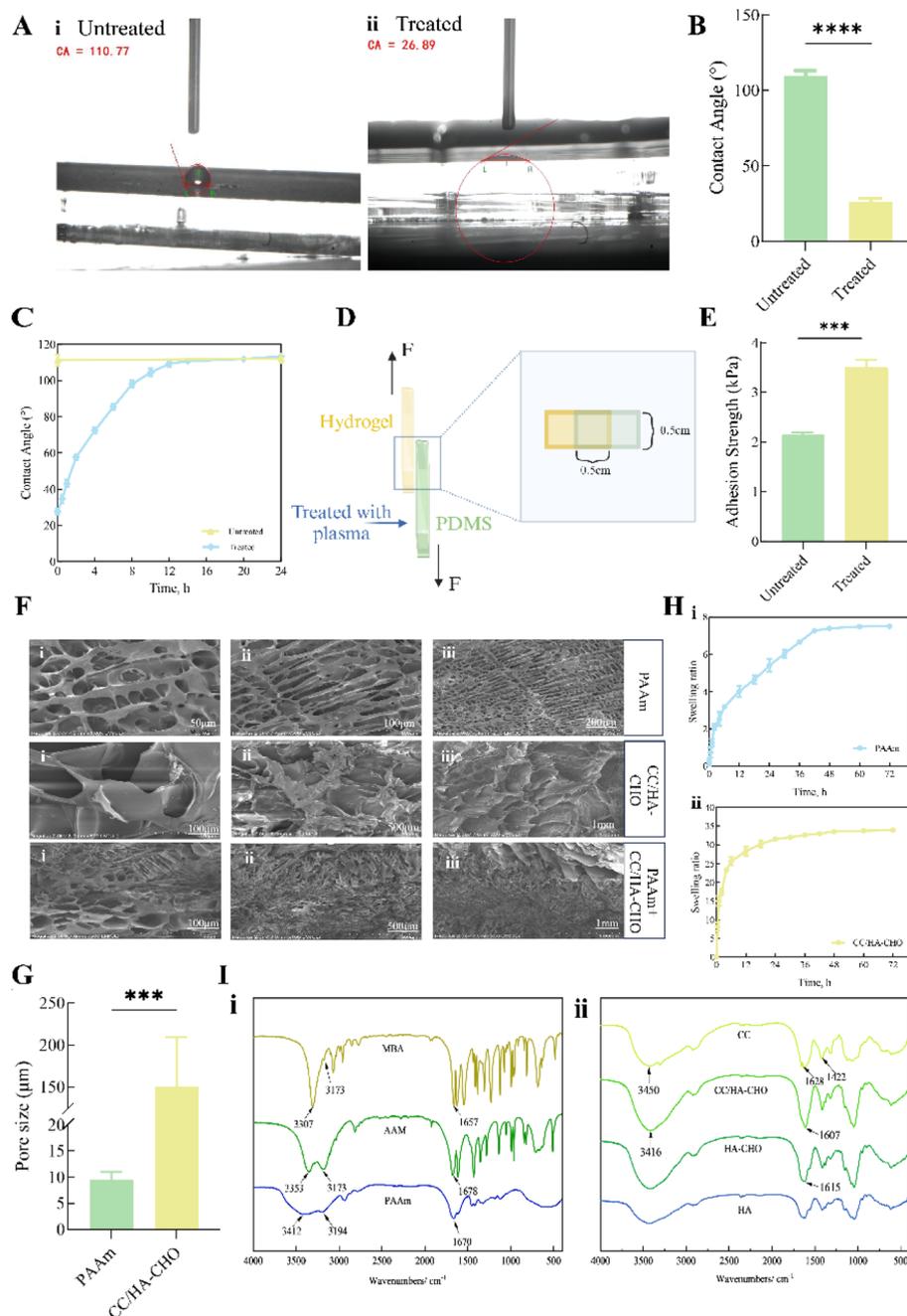
Fig. 2 Characterization of multilayer drug-loaded hydrogel. (A) Contact angle changes before (A, i) and after (A, ii) plasma treatment; (B) a *t*-test showed a significant difference in the contact angle before and after plasma treatment, ****$p < 0.0001$. Data are presented as mean $\pm$ SD ($n = 5$); (C) variation of the contact angle with time; (D) schematic diagram of the universal testing machine; (E) a *t*-test showed a significant difference in the adhesion force between PDMS and hydrogel after plasma treatment, ***$p < 0.001$. Data are presented as mean $\pm$ SD ($n = 5$); (F) microstructure of PAAm, CC/HA-CHO, and cross-sectional microstructure of both PAAm layer and CC/HA-CHO layer hydrogel observed by SEM; (G) a *t*-test showed a significant difference in the microstructural pore size across different layers of the hydrogel, ***$p < 0.001$; (H, i) swelling ratio of PAAm hydrogel over 48 hours; (H, ii) swelling ratio of CC/HA-CHO hydrogel over 48 hours; (I, i) FTIR analysis of CC/HA-CHO and constituent components; (I, ii) FTIR analysis of PAAm and constituent components.

method. Immersing the prepared hydrogel in PBS (pH = 7.4) after freeze-drying. At specified time points, remove the swollen hydrogel, blot excess surface water with filter paper, and weigh. The swelling ratio (SR) was calculated as:

$$\mathrm{SR}(\%) = \frac{M_s - M_d}{M_d} \times 100\%$$

where SR is the swelling ratio (%), M_s is the mass of the swollen hydrogel at a given time point (or at equilibrium), and M_d is the
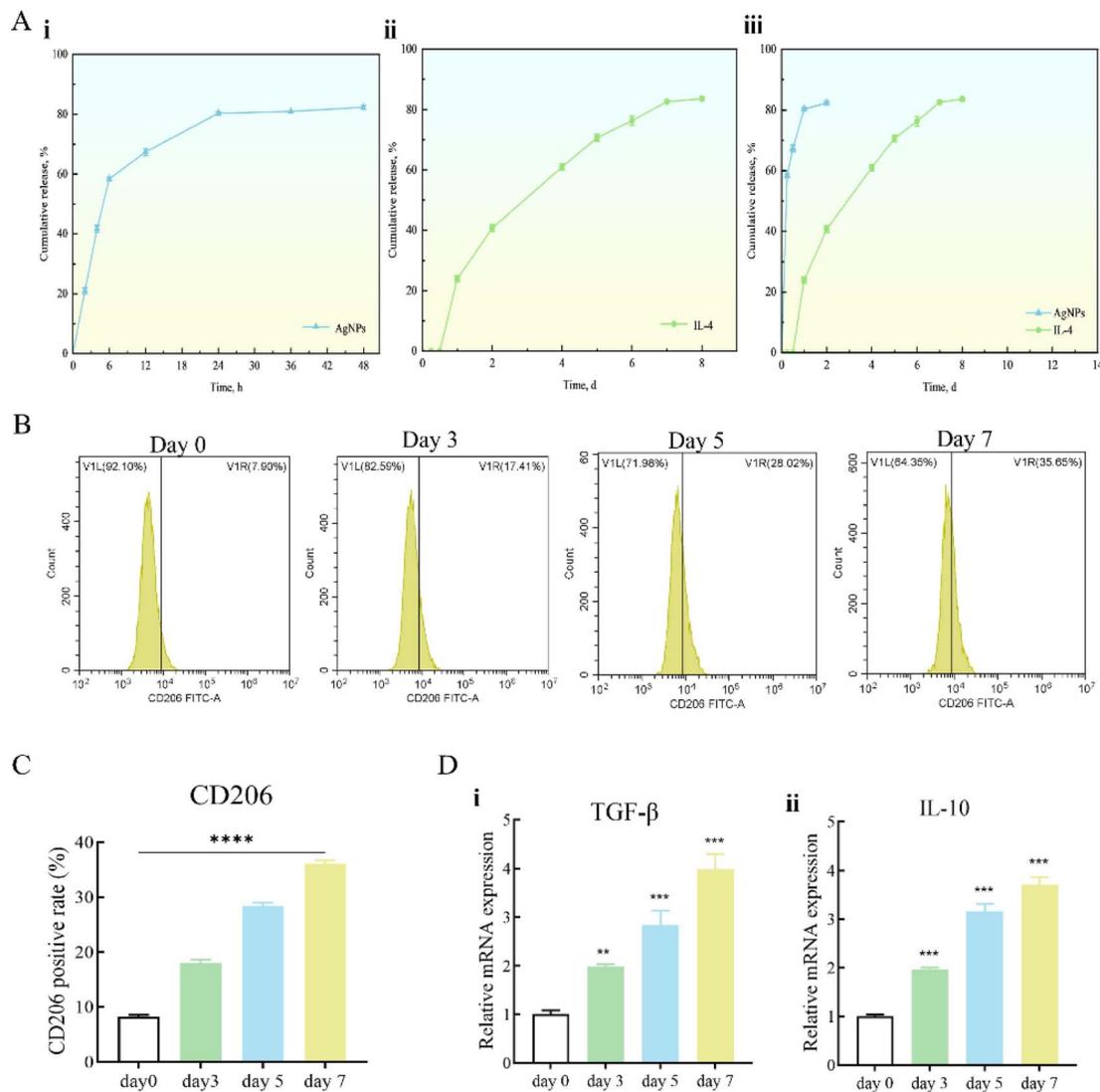
Fig. 3 Drug release experiment from multilayer drug-loaded hydrogel. (A, i) Cumulative release of AgNPs over 48 hours; (A, ii) cumulative release of IL-4 over 8 days; (A, iii) comparative release profiles of AgNPs *versus* IL-4; (B) *in vitro* detection of M2 macrophage surface marker CD206 by flow cytometry; (C) one-way ANOVA analysis of CD206-positive rates at different time points; (D) qPCR analysis of M2 macrophage transcriptional markers (IL-10 and TGF-β) at different time points.$**p < 0.01$, $***p < 0.001$, $****p < 0.0001$. Experiments were repeated in triplicate ($n = 3$).

mass of the dry hydrogel after drying to constant weight. All experiments were conducted in triplicate.

2.3.5 Microstructure of CC/HA-CHO hydrogel and PAAm hydrogel. After assembly, freeze-dry CC/HA-CHO hydrogel and PAAm hydrogel, then observe their microstructure including surface morphology and cross-section using scanning electron microscopy (SEM, S-4800, Hitachi®, Japan).

2.4 Drug release experiments

2.4.1 Drug release kinetics. Multilayer drug-loaded hydrogels were placed in modified syringes. PBS (pH = 7.4) was added to allow only the surface of AgNPs-loaded CC/HA-CHO hydrogel to contact the PBS, simulating the situation where only one surface of the dressing contacts the wound bed.[9] The concentration of IL-4 in the extraction fluid was measured using ELISA,

while the concentration of AgNPs was measured using UV-visible spectrophotometry (absorption peak at 400 nm, METASH®, China) over 14 days with daily replacement of fresh dispersion. We quantified release kinetics using model-independent descriptors, including burst release, T50 by linear interpolation, and mean dissolution/release time (MDT) by statistical moment analysis. Model-independent approaches are accepted for dissolution/release profile evaluation.[28]

2.4.2 Macrophage polarization regulation. Extraction fluid collected on days 3, 5, and 7 was used to culture RAW264.7 macrophages. Flow cytometry was used to detect surface marker CD206 of M2-type macrophages, and qPCR was used to detect transcription markers IL-10 and TGF-β to identify changes in macrophage polarization.
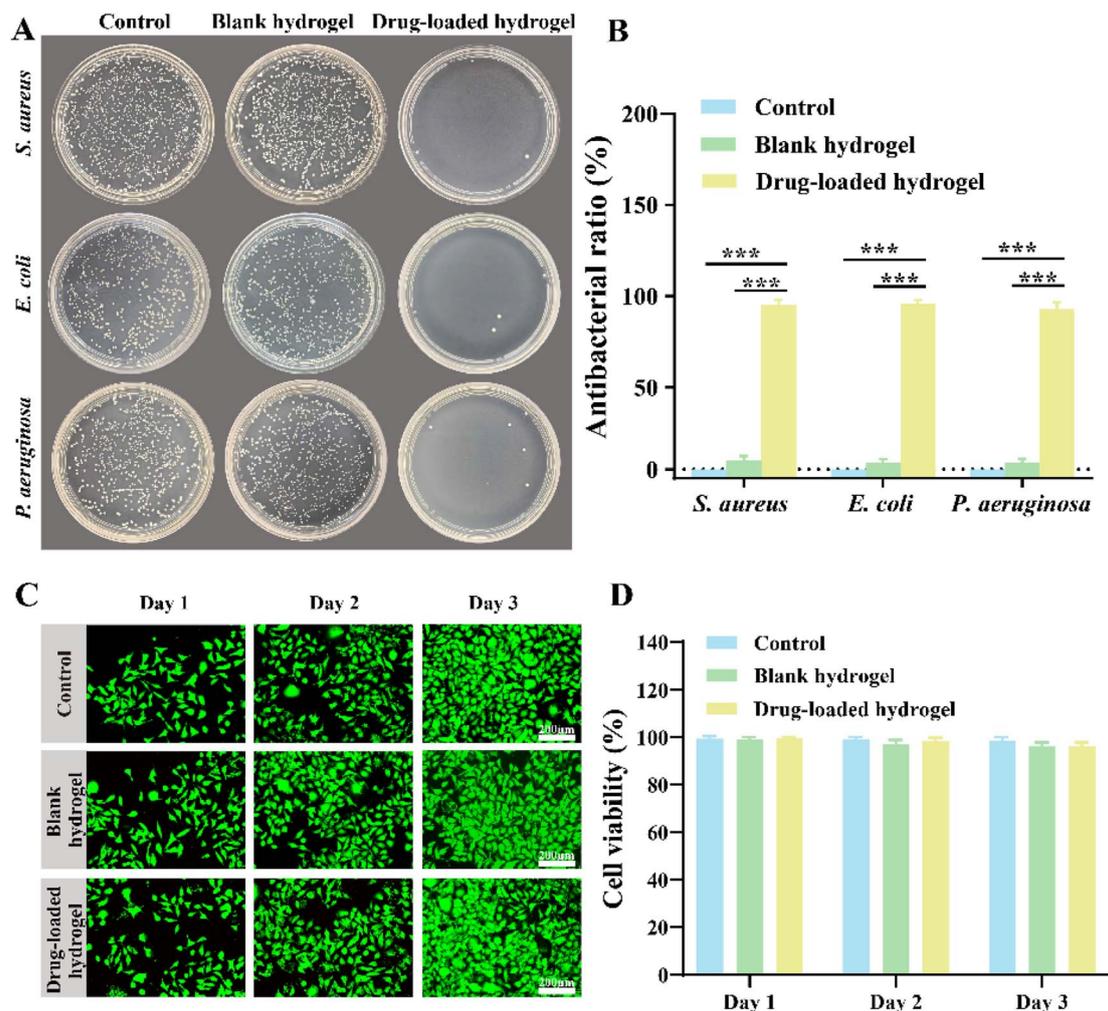
Fig. 4 *In vitro* antibacterial and biocompatibility studies. (A) Antibacterial performance against *S. aureus*, *E. coli*, and *P. aeruginosa* in the control, blank hydrogel, and drug-loaded hydrogel groups; (B) one-way ANOVA analysis of the antibacterial activity in each group ($n = 3$); (C) fluorescent live/dead staining images of L929 cells cultured with different hydrogels; green fluorescence indicates live cells and red fluorescence indicates dead cells; (D) L929 cell viability after treatment with each hydrogel group ($n = 6$). ***$p < 0.001$.

2.5   Antibacterial assay *in vitro*

We obtained PBS extracts from blank hydrogel and drug-loaded hydrogel respectively, with pure PBS serving as the control group. According to the McFarland standard, bacterial suspensions of *Staphylococcus aureus* (*S. aureus*), *Escherichia coli* (*E. coli*), and *Pseudomonas aeruginosa* (*P. aeruginosa*) were prepared to a turbidity of 0.5. Then, 200 μL of each bacterial suspension was added to 5 mL of liquid LB medium. Each bacterial culture was mixed with an equal volume (1 : 1 ratio) of the corresponding PBS solution from each group, followed by shaking incubation at 37 °C for 6 hours. Finally, 100 μL of the diluted bacterial solution was spread onto LB agar plates and incubated at 37 °C for 24 hours, after which photographs were taken and colony-forming units (CFU) were counted.[9]

2.6   Cytocompatibility assay

The CCK-8 assay was employed to evaluate the *in vitro* biocompatibility of the multilayer drug-loaded hydrogel with

L929 cells. DMEM medium extracts were obtained from the blank hydrogel and the drug-loaded hydrogel, respectively, with plain DMEM medium serving as the control. These DMEM media were then supplemented with 10% fetal bovine serum to prepare complete culture media. L929 cells were seeded in a 96-well plate at a density of 3×10^3 cells per well and cultured for 24 hours. After removing the culture medium, the cells were washed three times with PBS, and 10 μL of CCK-8 reagent (Cell Counting Kit-8, Beyotime Biotechnology Co. Ltd, Beijing, China) was added to each well, followed by incubation for 1 hour. Absorbance was measured at 450 nm using a microplate reader (Bio Tek, USA). The same procedure was performed to assess cell viability on the second and third days of culture ($n = 6$). The cell viability was calculated as:

$$\text{Cell viability}(\%) = \frac{A_{\text{sample}} - A_{\text{medium}}}{A_{\text{control}} - A_{\text{medium}}} \times 100$$

where, A_{sample} and A_{control} represent the absorbance of cells treated with the hydrogel extract and untreated cells,
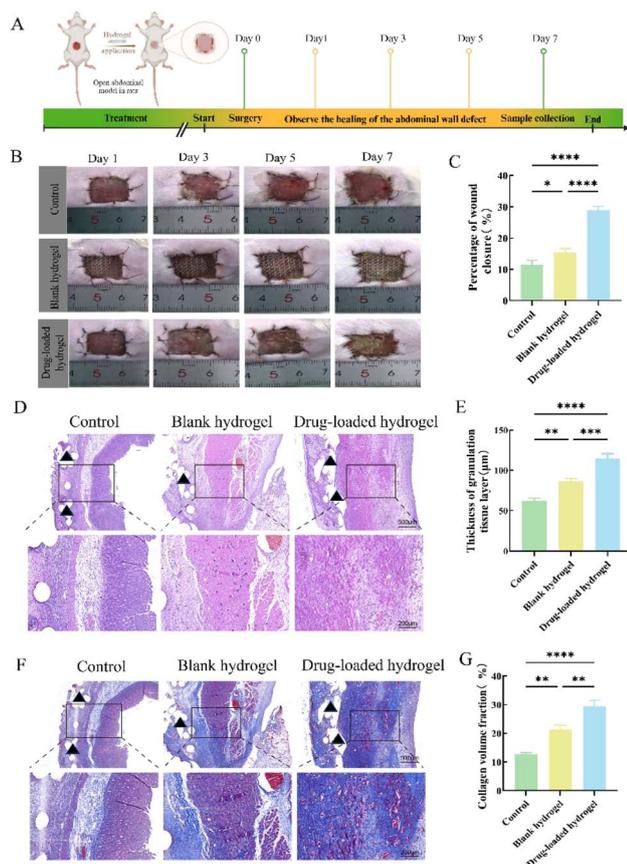
Fig. 5 Multi-layer drug-loaded hydrogel animal study. (A) Schematic diagram of the animal experiment. (B) Images of abdominal wound healing in rats under different interventions. (C) One-way ANOVA analysis of the percentage of abdominal wound healing area under different interventions. (D) Comparison of granulation tissue regeneration and inflammatory cell infiltration among groups by HE staining. (E) One-way ANOVA analysis of granulation tissue thickness under different interventions. (F) Comparison of collagen fiber regeneration by Masson staining. (G) One-way ANOVA analysis of collagen fiber content under different interventions. *, $p < 0.05$; **, $p < 0.01$; ***, $p < 0.001$; ****, $p < 0.0001$. The black triangular areas in the images indicate the hydrogel regions. The sample size per group was 6 ($n = 6$).

respectively, while A_{medium} denotes the absorbance of the culture medium without cells.[29,30]

Furthermore, live/dead cell staining was performed to assess cell viability. Specifically, DMEM extracts of blank hydrogel and drug-loaded hydrogel were prepared, with plain DMEM used as the control. Each extract was supplemented with 10% fetal bovine serum to obtain complete culture media. L929 cells were seeded in a 96-well plate at a density of 3×10^3 cells per well. At 24, 48, and 72 hours, the cells were stained using a diluted live/dead staining reagent (Calcein AM/PI/Hoechst Cell Viability Assay Kit, Beyotime Biotechnology Co. Ltd, Beijing, China). For each well, 100 μL of diluted Calcein AM and 100 μL of diluted propidium iodide (PI) were added, followed by incubation for 10 minutes. Fluorescent images were acquired using an inverted fluorescence microscope (Leica, Germany).[29,30]

2.7 Construction of rat open abdomen wound model

2.7.1 Animal preparation. Eighteen SPF-grade male SD rats weighing 210–250 g were randomly divided into three groups: no hydrogel group (control group), blank hydrogel group, and drug-loaded hydrogel group. Rats were housed individually under controlled conditions (23 ± 2 °C, 50 ± 10% relative humidity, 12-hour light/dark cycle) with free access to food and water. Before surgery, rats were fasted for 12 hours with free access to water. Animal experiments were conducted following the guidelines for the care and use of laboratory animals (Ministry of Science and Technology of China [2006] No. 398 document) and approved by the Ethics Committee of Nanjing Medical University.

2.7.2 Experimental procedure. Rats were anesthetized deeply with 3% pentobarbital sodium at a dose of 60 mg kg^{-1} and shaved in the abdominal area. A 1.5×1.5 cm square was marked and the abdominal skin was incised along the mark. After entering the abdominal cavity, the abdominal wall was excised to create a 1.5 cm × 1.5 cm abdominal defect. In the control group, the skin was sutured directly with polypropylene mesh. In the blank hydrogel and drug-loaded hydrogel groups, hydrogel dressings were placed on the wound bed before suturing the skin with polypropylene mesh. After modeling, rats were intramuscularly injected with procaine penicillin for the first 3 days. Rats were closely monitored, including body weight, activity, food and water intake, and clinical signs related to wound infection, and no unexpected adverse events were observed. On days 1, 3, 5, and 7, wound healing was observed and photographed with a scale. After 7 days of model establishment, fresh granulation tissue will be collected from two animals in each group for flow cytometry analysis, and wound healing tissue will be fixed from four animals in each group for histological analysis. HE staining will be used to detect pathological changes in wound healing tissue, and Masson staining will be used to detect collagen changes in wound healing tissue. Infiltrating macrophages will be isolated, and flow cytometry will be used to detect the surface marker CD206 for macrophage polarization. qPCR will be used to detect transcriptional markers IL-10 and TGF-β for macrophage polarization. Immunofluorescence staining will be used to observe the content and distribution of macrophage markers CD206 in granulation tissue.[31]

2.8 Statistical analysis

Statistical analysis was performed using OriginPro 2024b and Graphpad Prism 10 software. The t-test or one-way ANOVA analysis was used to compare differences between groups, and $p < 0.05$ was considered statistically significant. Results are presented as mean ± SD.

3. Results and discussion

3.1 Hydrogel characterization

PDMS itself is hydrophobic,[32] so we first evaluated the hydrophilicity of PDMS after plasma treatment. Before treatment, the contact angle was $109.34 \pm 3.74°$ (mean ± SD, $n = 5$), which
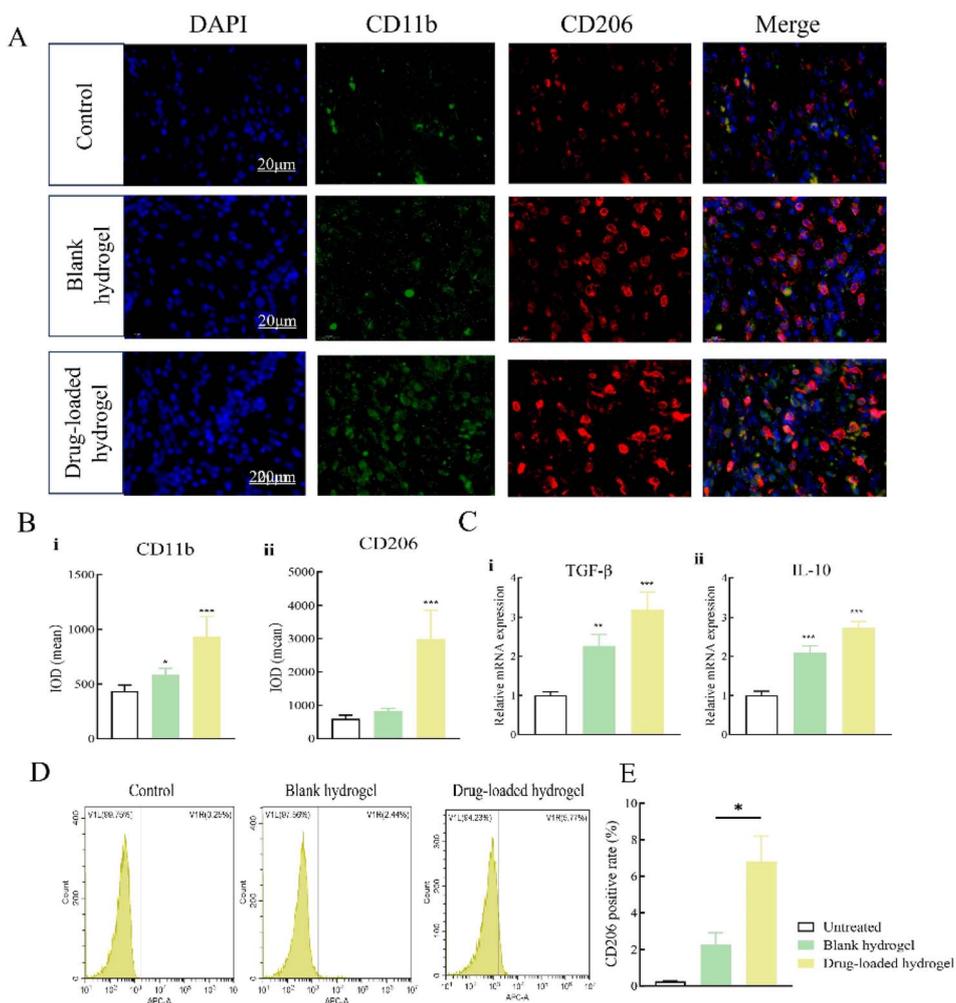
Fig. 6 Analysis of macrophage polarization in animal experiments. (A) Immunofluorescence staining images of CD206, a surface marker of M2 macrophages, under different intervention modes; (B) one-way ANOVA analysis of fluorescence intensity among groups; (C) qPCR analysis of M2 macrophage polarization transcriptional markers IL-10 and TGF-β expression levels in each group; (D) flow cytometry detection of M2 macrophage polarization surface marker CD206; (E) one-way ANOVA analysis of CD206-positive rates under different intervention modes. *, $p < 0.05$; **, $p < 0.01$; ***, $p < 0.001$. Experiments were repeated three times ($n = 3$).

decreased to $26.18 \pm 2.39°$ (mean $\pm$ SD, $n = 5$) after treatment (Fig. 2A), with statistically significant differences (Fig. 2B), indicating a transformation from hydrophobic to hydrophilic due to plasma treatment, the most commonly used method for PDMS surface modification.[33] However, a significant challenge post plasma treatment is the recovery of hydrophobicity (Fig. 2C), primarily due to uncured PDMS oligomers migrating to the surface and highly mobile polymer chains with Si–OH bonds rearranging towards the bulk at room temperature.[12] Moreover, the low glass transition temperature of PDMS (approximately -120 °C) exacerbates these effects.[33] Previous studies have shown that PAAm can graft polymerize effectively onto modified PDMS surfaces under UV irradiation and maintain stability for up to one month under dry room conditions.[34] To address the issue of hydrophobic recovery in PDMS, UV lamp irradiation was used to graft PAAm onto the modified PDMS surface in this study. Previous research indicates that the adhesive strength between modified PDMS and hydrogels

increases over time.[12] Therefore, we used a universal mechanical tester to measure the adhesive strength between PDMS and hydrogels before and after plasma treatment (Fig. 2D). The adhesive strength of PDMS to hydrogels significantly increased after plasma treatment compared to untreated PDMS (Fig. 2E) ($p < 0.001$).

One of the most critical parameters affecting drug release behavior is the surface structure of the drug carrier.[35] We observed the microstructure of the hydrogels using scanning electron microscopy (SEM), revealing a porous structure. The PAAm hydrogel exhibited a dense pore structure with thick walls, whereas the CC/HA-CHO hydrogel had a loose pore structure with thinner walls (Fig. 2F and G). This highly cross-linked microporous structure not only accommodates various cells but also facilitates the release of various drugs and other nano-trace elements effectively.[8]

The hydrogel exhibited rapid water absorption within the first 12 hours, followed by a slower swelling rate after 18 hours

Paper

RSC Advances

(Fig. 2H). The swelling ratio of PAAm was approximately 750%, while CC/HA-CHO exhibited a high swelling ratio of up to 3300%. It is well known that the swelling ratio of hydrogels is closely related to pore size and hydrophilicity.[36,37] CC/HA-CHO hydrogel has larger pores, providing more space for water absorption (Fig. 2G). Additionally, HA-CHO introduces –COOH groups in the gel, which converts to COO– in alkaline environments, increasing repulsive forces between like charges. Thus, CC/HA-CHO hydrogel rapidly swells in alkaline solutions at pH = 7.4, beneficial for absorbing wound exudate and maintaining a moist wound environment.[38]

We confirmed the chemical structure of the PAAm hydrogel using FTIR (Fig. 2I). Characteristic absorption peaks corresponding to $-NH_2$ appeared at 3412 cm^{-1} and 3194 cm^{-1}, while peaks corresponding to $-C=O$ appeared at 1670 cm^{-1}, confirming the successful preparation of PAAm hydrogel.[39,40] Furthermore, we analyzed the FTIR spectra of CC/HA-CHO, where absorption peaks at 3450 cm^{-1} were attributed to hydroxyl and amino stretching vibrations.[41] Peaks corresponding to asymmetric and symmetric carboxylate stretching vibrations appeared at 1628 cm^{-1} and 1422 cm^{-1}, respectively.[42] The appearance of absorption peaks at 1615 cm^{-1} is primarily due to the introduction of aldehyde groups in the structure of HA, and the decrease in peaks at 1615 cm^{-1} and 3450 cm^{-1} after mixing CC and HA-CHO confirms the Schiff base crosslinking reaction between amino and aldehyde groups.[43]

3.2 Investigation of drug release patterns in drug-loaded hydrogels

We quantified the concentrations of AgNPs and IL-4 in extraction fluids using UV-visible spectrophotometry and ELISA, respectively (Fig. 3A). AgNPs began releasing from the second hour, reaching equilibrium concentration by the second day. IL-4 release started from the first day and reached equilibrium concentration by the eighth day, showing a delayed release compared to AgNPs, likely due to barrier effects.[9] For AgNPs, the burst release at 2 h was 21.68%, T50 was 4.96 h, the MDT was 6.20 h. For IL-4, burst release was 24.95% at 1 day, T50 was 2.99 days, the MDT was 2.71 days. These results quantitatively support the intended sequential release behavior. The larger pore size and faster release rate of CC/HA-CHO hydrogel might contribute to this delay. Early release of AgNPs can achieve early antimicrobial effects.

Furthermore, IL-4 exhibited a longer release duration than AgNPs. Previous studies have shown that incorporating various insoluble nanoparticles such as ZnO, CuO, Ag, Au into hydrogel matrices can improve mechanical properties, antimicrobial performance, and stability, as well as regulate drug release rates, prolonging drug release times.[44,45] Therefore, the prolonged release of IL-4 may be attributed to the presence of AgNPs in the hydrogel base layer, which is beneficial for tissue wound repair. Thus, the multi-layered drug-loaded hydrogel can achieve sequential drug release, showing great potential as a wound dressing for wound repair.

3.3 Regulation of macrophage polarization

We cultured RAW264.7 macrophages in extraction fluids collected at different time points (days 3, 5, and 7). We first examined the expression level of the M2 macrophage surface marker CD206 using flow cytometry. The results showed that CD206 expression progressively increased on days 3, 5, and 7 (Fig. 3B). Furthermore, one-way ANOVA analysis revealed significant differences in CD206 expression levels (Fig. 3C). Therefore, the multilayer drug-loaded hydrogel promotes macrophage polarization towards the M2 phenotype by releasing IL-4. Additionally, we detected M2-type macrophage transcription markers IL-10 and TGF-β using qPCR.[24] The expression levels of IL-10 and TGF-β gradually increased on days 3, 5, and 7, further validating the ability of the multilayer drug-loaded hydrogel to promote M2 polarization in macrophages (Fig. 3D).

3.4 Antibacterial property of drug-loaded hydrogel

The antibacterial performance of the multilayer drug-loaded hydrogel was evaluated. Due to the incorporation of AgNPs within the CC/HA-CHO hydrogel layer, this drug-loaded hydrogel demonstrated strong antibacterial activity against *S. aureus*, *E. coli*, and *P. aeruginosa* (Fig. 4A and B). These results suggest that this drug-loaded hydrogel can effectively exert antibacterial effects during wound healing.

3.5 Biocompatibility of drug-loaded hydrogel

The multilayer drug-loaded hydrogel was expected to exhibit favorable biocompatibility, which was evaluated using the L929 cells. Live/dead staining results showed that nearly no dead cells were observed on days 1, 2, and 3, while the number of cells increased over time in all groups (Fig. 4C). Furthermore, CCK-8 assays indicated no statistically significant differences in cell viability between the control group and the hydrogel groups on days 1, 2, and 3 (Fig. 4D). Therefore, this multilayer drug-loaded hydrogel demonstrates excellent biocompatibility.

3.6 Drug-loaded hydrogel promotes wound healing

We divided the experimental animals into three groups: control group, blank hydrogel group, and drug-loaded hydrogel group. The healing progress of abdominal wounds was compared among the three groups on days 1, 3, 5, and 7 (Fig. 5A). The drug-loaded hydrogel group exhibited significantly faster wound healing, characterized by the gradual formation of a dry, yellow-brown thin scab. In contrast, the other two groups showed slower healing (Fig. 5B and C). On day 7, tissue surrounding the abdominal wall defects was collected and fixed overnight in 10% neutral formalin. Histopathological changes were evaluated using HE and Masson staining.

The HE staining results from the drug-loaded hydrogel group demonstrated superior wound closure and a more uniform distribution of fibrous tissue, indicating enhanced tissue reconstruction. Furthermore, there was a marked reduction in inflammatory cell infiltration, suggesting suppression of the local inflammatory response. Additionally,

angiogenesis was significantly enhanced, improving the wound healing environment (Fig. 5D and E). The Masson staining results showed that the drug-loaded hydrogel group exhibited the best healing outcomes, effectively promoting tissue reconstruction through enhanced collagen deposition and angiogenesis (Fig. 5F and G).

Macrophages were isolated from the abdominal wall defect tissues, and surface markers of macrophage polarization, such as CD206, were assessed using qPCR, flow cytometry and immunofluorescence staining. The drug-loaded hydrogel group exhibited the strongest CD206 immunofluorescence staining, suggesting the greatest M2 macrophage polarization (Fig. 6A and B). Transcriptional markers of macrophage polarization, including IL-10 and TGF-β, were also detected using qPCR. The results demonstrated significantly elevated expression of IL-10 and TGF-β in the drug-loaded hydrogel group, with statistical significance confirmed by one-way ANOVA analysis (Fig. 6C). Flow cytometry analysis revealed that the drug-loaded hydrogel group exhibited the highest CD206$^+$ cell ratio, demonstrating the strongest M2 macrophage polarization (Fig. 6D and E). These findings suggest that the drug-loaded hydrogel promotes macrophage polarization towards the M2 phenotype at the wound site. Therefore, this animal study demonstrates that drug-loaded hydrogels can alleviate inflammation at open abdominal wound sites and significantly accelerate wound healing.

However, in this section, we did not include a comparative study between the multilayer drug-loaded hydrogel and standard commercial OA wound dressings such as negative-pressure wound therapy (NPWT) foam and standard biologic mesh.[46] Therefore, this indeed constitutes a major limitation of our current study. In future research, we will supplement a detailed comparison plan against NPWT-based temporary abdominal closure. Previous studies have also reported a double-layered bioadhesive patch (hydrogel + tough antibacterial polyurethane film) designed for rapid hemostasis and suture-free sealing of acute bleeding wounds, which provides a relevant benchmark for high-strength sealing materials.[47] However, it addresses a clinical scenario different from temporary abdominal closure in OA cases. In summary, the multilayer drug-loaded hydrogel in our study serves as a complement to standard commercial OA wound dressings, aiming to provide dual anti-inflammatory and pro-healing therapy for OA wounds.

In addition, hematological blood parameters (*e.g.*, complete blood count with differential) were not performed in this animal experiment. In future studies, we will include these parameters to further strengthen the assessment of systemic inflammatory status and overall safety.

4. Conclusion

In this study, we designed and fabricated a multilayer drug-loaded hydrogel dressing for the protection of open abdominal wounds. By integrating the antibacterial of CC/HA-CHO hydrogels, the controlled drug-release characteristics of PAAm hydrogels, and the excellent antifouling capability of PDMS, we developed a functional structure with distinct layers. In the drug-loading strategy, AgNPs were employed for early-stage antibacterial and anti-infective effects, while IL-4 facilitated macrophage polarization towards the M2 phenotype during the tissue repair phase, providing robust regenerative support for the wound.

The multilayer structure and multifunctional design of the dressing address the critical requirements of open abdominal wounds, including a moist environment, antibacterial activity, and biocompatibility. Moreover, its capability for gradual and targeted drug release offers a novel approach for precise control over wound healing. Material characterization and *in vitro* experiments demonstrated the hydrogel dressing's strong adhesive strength, mechanical stability, and effective drug release performance.

Based on these initial findings, the multilayer drug-loaded hydrogel dressing shows significant potential for application in open abdominal therapy, offering an innovative solution for managing severe abdominal trauma and complex infected wounds. However, further animal studies and clinical research are necessary to validate its safety and efficacy in practical applications, providing valuable guidance for advancing this field.

Author contributions

Study concept and design: T. Z., Y. Z. and J. H. Data acquisition, analysis and interpretation: R. W., K. C., Y. Y., G. Q., H. N., H. L., and R. W. Drafting of the manuscript: R. W. and K. C. Critical revision of the manuscript for important intellectual content: J. H., T. Z., and Y. Z. All authors read and approved the final manuscript.

Conflicts of interest

The authors declare that they have no competing interests.

Data availability

The datasets used and/or analysed during the current study are available from the corresponding author on reasonable request.

Supplementary information (SI) is available. See DOI: https://doi.org/10.1039/d5ra09472k.

Acknowledgements

References

1 F. Coccolini, M. Sartelli, R. Sawyer, *et al.*, Source control in emergency general surgery: WSES, GAIS, SIS-E, SIS-A guidelines, *World J. Emerg. Surg.*, 2023, **18**(1), 41.
2 A. W. Kirkpatrick, D. J. Roberts, J. De Waele, *et al.*, Intra-abdominal hypertension and the abdominal compartment syndrome: updated consensus definitions and clinical

practice guidelines from the World Society of the Abdominal Compartment Syndrome, *Intensive Care Med.*, 2013, **39**(7), 1190–1206.

3 F. Prete, G. M. De Luca, A. Pasculli, *et al.*, Retrospective Study of Indications and Outcomes of Open Abdomen with Negative Pressure Wound Therapy Technique for Abdominal Sepsis in a Tertiary Referral Centre, *Antibiotics*, 2022, **11**(11), 1498.

4 Y. Zhao, X. Li, N. Sun, *et al.*, Injectable Double Crosslinked Hydrogel-Polypropylene Composite Mesh for Repairing Full-Thickness Abdominal Wall Defects, *Adv. Healthcare Mater.*, 2024, e2304489.

5 A. Nishiguchi, S. Ito, K. Nagasaka and T. Taguchi, Tissue-Adhesive Decellularized Extracellular Matrix Patches Reinforced by a Supramolecular Gelator to Repair Abdominal Wall Defects, *Biomacromolecules*, 2023, **24**(4), 1545–1554.

6 R. Sanz-Horta, A. Matesanz, A. Gallardo, *et al.*, Technological advances in fibrin for tissue engineering, *J. Tissue Eng.*, 2023, **14**, 20417314231190288.

7 Y. Liang, J. He and B. Guo, Functional Hydrogels as Wound Dressing to Enhance Wound Healing, *ACS Nano*, 2021, **15**(8), 12687–12722.

8 T. Xiang, Q. Guo, L. Jia, *et al.*, Multifunctional Hydrogels for the Healing of Diabetic Wounds, *Adv. Healthcare Mater.*, 2024, **13**(1), e2301885.

9 T. Zheng, J. Huang, Y. Jiang, *et al.*, Sandwich-structure hydrogels implement on-demand release of multiple therapeutic drugs for infected wounds, *RSC Adv.*, 2019, **9**(72), 42489–42497.

10 H. Guo, C. Wen, S. Tian, *et al.*, Universal Intraductal Surface Antifouling Coating Based on an Amphiphilic Copolymer, *ACS Appl. Mater. Interfaces*, 2021, **13**(18), 21051–21059.

11 T. Wu, Y. Qi, Q. Chen, C. Gu and Z. Zhang, Preparation and Properties of Fluorosilicone Fouling-Release Coatings, *Polymers*, 2022, **14**(18), 3804.

12 K. Tian, J. Bae, Z. Suo and J. J. Vlassak, Adhesion between Hydrophobic Elastomer and Hydrogel through Hydrophilic Modification and Interfacial Segregation, *ACS Appl. Mater. Interfaces*, 2018, **10**(49), 43252–43261.

13 H. Li, F. Cheng, X. Wei, *et al.*, Injectable, self-healing, antibacterial, and hemostatic N,O-carboxymethyl chitosan/oxidized chondroitin sulfate composite hydrogel for wound dressing, *Mater. Sci. Eng., C*, 2021, **118**, 111324.

14 L. Zhang, B. Luo, Z. An, *et al.*, MMP-Responsive Nanoparticle-Loaded, Injectable, Adhesive, Self-Healing Hydrogel Wound Dressing Based on Dynamic Covalent Bonds, *Biomacromolecules*, 2023, **24**(12), 5769–5779.

15 S. Li, Q. Dong, X. Peng, *et al.*, Self-Healing Hyaluronic Acid Nanocomposite Hydrogels with Platelet-Rich Plasma Impregnated for Skin Regeneration, *ACS Nano*, 2022, **16**(7), 11346–11359.

16 H. Chen, F. Fei, X. Li, *et al.*, A structure-supporting, self-healing, and high permeating hydrogel bioink for establishment of diverse homogeneous tissue-like constructs, *Bioact. Mater.*, 2021, **6**(10), 3580–3595.

17 F. Zhang, S. Zhang, R. Lin, S. Cui, X. Jing and S. Coseri, Injectable multifunctional carboxymethyl chitosan/hyaluronic acid hydrogel for drug delivery systems, *Int. J. Biol. Macromol.*, 2023, **249**, 125801.

18 K. Tian, Z. Suo and J. J. Vlassak, Chemically Coupled Interfacial Adhesion in Multimaterial Printing of Hydrogels and Elastomers, *ACS Appl. Mater. Interfaces*, 2020, **12**(27), 31002–31009.

19 L. Xu, Y. Y. Wang, J. Huang, C. Y. Chen, Z. X. Wang and H. Xie, Silver nanoparticles: Synthesis, medical applications and biosafety, *Theranostics*, 2020, **10**(20), 8996–9031.

20 A. Hassanshahi, M. Moradzad, S. Ghalamkari, M. Fadaei, A. J. Cowin and M. Hassanshahi, Macrophage-Mediated Inflammation in Skin Wound Healing, *Cells*, 2022, **11**(19), 2953.

21 H. Al Sadoun, Macrophage Phenotypes in Normal and Diabetic Wound Healing and Therapeutic Interventions, *Cells*, 2022, **11**(15), 2430.

22 S. M. Aitcheson, F. D. Frentiu, S. E. Hurn, K. Edwards and R. Z. Murray, Skin Wound Healing: Normal Macrophage Function and Macrophage Dysfunction in Diabetic Wounds, *Molecules*, 2021, **26**(16), 4917.

23 M. Sharifiaghdam, E. Shaabani, R. Faridi-Majidi, S. C. De Smedt, K. Braeckmans and J. C. Fraire, Macrophages as a therapeutic target to promote diabetic wound healing, *Mol. Ther.*, 2022, **30**(9), 2891–2908.

24 Y. Yao, X. H. Xu and L. Jin, Macrophage Polarization in Physiological and Pathological Pregnancy, *Front. Immunol.*, 2019, **10**, 792.

25 J. Huang, J. Ren, G. Chen, *et al.*, Tunable sequential drug delivery system based on chitosan/hyaluronic acid hydrogels and PLGA microspheres for management of non-healing infected wounds, *Mater. Sci. Eng., C*, 2018, **89**, 213–222.

26 T. Nakajima, K. Mito and J. P. Gong, Mechanical Model for Super-Anisotropic Swelling of the Multi-Cylindrical PDGI/PAAm Gels, *Polymers*, 2023, **15**(7), 1624.

27 A. Borók, K. Laboda and A. Bonyár, PDMS Bonding Technologies for Microfluidic Applications: A Review, *Biosensors*, 2021, **11**(8), 292.

28 D. A. Diaz, S. T. Colgan, C. S. Langer, N. T. Bandi, M. D. Likar and L. Van Alstine, Dissolution Similarity Requirements: How Similar or Dissimilar Are the Global Regulatory Expectations?, *AAPS J.*, 2016, **18**(1), 15–22.

29 Y. H. Chen, Z. F. Rao, Y. J. Liu, X. S. Liu, Y. F. Liu, L. J. Xu, Z. Q. Wang, J. Y. Guo, L. Zhang, Y. S. Dong, C. X. Qi, C. Yang, S. F. Wang, *et al.*, Multifunctional Injectable Hydrogel Loaded with Cerium-Containing Bioactive Glass Nanoparticles for Diabetic Wound Healing, *Erratum in: Biomolecules*, 2024, **14**(3), 283, DOI: 10.3390/biom11050702.

30 Q. Zong, X. Peng, Y. Ding, *et al.*, Multifunctional hydrogel wound dressing with rapid on-demand degradation property based on aliphatic polycarbonate and chitosan, *Int. J. Biol. Macromol.*, 2023, **244**, 125138.

31 Y. Liu, S. Li, J. Huang, *et al.*, Establishment and evaluation of an improved rat model of open abdomen, *Anim. Models Exp. Med.*, 2024, **7**(4), 562–569.

32 J. Zhang, Y. Huang, X. Zhang, *et al.*, Flexible transparent and hydrophobic SiNCs/PDMS coatings for anti-counterfeiting applications, *Mater. Horiz.*, 2024, **11**(15), 3573–3584.

33 J. Zhou, A. V. Ellis and N. H. Voelcker, Recent developments in PDMS surface modification for microfluidic devices, *Electrophoresis*, 2010, **31**(1), 2–16.

34 D. Xiao, H. Zhang and M. Wirth, Chemical Modification of the Surface of Poly(dimethylsiloxane) by Atom-Transfer Radical Polymerization of Acrylamide, *Langmuir*, 2002, **18**(25), 9971–9976.

35 Z. Zare-Akbari, H. Farhadnejad, B. Furughi-Nia, S. Abedin, M. Yadollahi and M. Khorsand-Ghayeni, PH-sensitive bionanocomposite hydrogel beads based on carboxymethyl cellulose/ZnO nanoparticle as drug carrier, *Int. J. Biol. Macromol.*, 2016, **93**(Pt A), 1317–1327.

36 H. Sun, M. Zhang, M. Liu, Y. Yu, X. Xu and J. Li, Fabrication of Double-Network Hydrogels with Universal Adhesion and Superior Extensibility and Cytocompatibility by One-Pot Method, *Biomacromolecules*, 2020, **21**(12), 4699–4708.

37 Q. Zhang, X. M. Hu, M. Y. Wu, M. M. Wang, Y. Y. Zhao and T. T. Li, Synthesis and performance characterization of poly(vinyl alcohol)-xanthan gum composite hydrogel, *React. Funct. Polym.*, 2019, **136**, 34–43.

38 S. Zhang, L. Kang, S. Hu, *et al.*, Carboxymethyl chitosan microspheres loaded hyaluronic acid/gelatin hydrogels for controlled drug delivery and the treatment of inflammatory bowel disease, *Int. J. Biol. Macromol.*, 2021, **167**, 1598–1612.

39 S. Tang, Z. Gong, Z. Wang, X. Gao and X. Zhang, Multifunctional hydrogels for wound dressings using xanthan gum and polyacrylamide, *Int. J. Biol. Macromol.*, 2022, **217**, 944–955.

40 T. S. Sorkhabi, M. F. Samberan, K. A. Ostrowski, T. M. Majka, M. Piechaczek and P. Zajdel, Preparation and Characterization of Novel Microgels Containing Nano-SiO(2) and Copolymeric Hydrogel Based on Poly (Acrylamide) and Poly (Acrylic Acid): Morphological, Structural and Swelling Studies, *Materials*, 2022, **15**(14), 4782.

41 Z. Liu, X. Mo, F. Ma, *et al.*, Synthesis of carboxymethyl chitosan-strontium complex and its therapeutic effects on relieving osteoarthritis, *Carbohydr. Polym.*, 2021, **261**, 117869.

42 Q. K. Zhong, Z. Y. Wu, Y. Q. Qin, *et al.*, Preparation and Properties of Carboxymethyl Chitosan/Alginate/Tranexamic Acid Composite Films, *Membranes*, 2019, **9**(1), 11.

43 M. Du, J. Jin, F. Zhou, J. Chen and W. Jiang, Dual drug-loaded hydrogels with pH-responsive and antibacterial activity for skin wound dressing, *Colloids Surf., B*, 2023, **222**, 113063.

44 Y. Li, X. E. Luo, M. J. Tan, *et al.*, Preparation of carboxymethylcellulose/ZnO/chitosan composite hydrogel microbeads and its drug release behaviour, *Int. J. Biol. Macromol.*, 2023, **247**, 125716.

45 B. Rashidzadeh, E. Shokri, G. R. Mahdavinia, R. Moradi, S. Mohamadi-Aghdam and S. Abdi, Preparation and characterization of antibacterial magnetic-/pH-sensitive alginate/Ag/Fe(3)O(4) hydrogel beads for controlled drug release, *Int. J. Biol. Macromol.*, 2020, **154**, 134–141.

46 F. Coccolini, D. Roberts, L. Ansaloni, *et al.*, The open abdomen in trauma and non-trauma patients: WSES guidelines, *World J. Emerg. Surg.*, 2018, **13**, 7.

47 Z. Zeng, J. Zhang, Y. Gao, *et al.*, Bioadhesive First-Aid Patch with Rapid Hemostasis and High Toughness Designed for Sutureless Sealing of Acute Bleeding Wounds, *Adv. Healthcare Mater.*, 2025, **14**(2), e2403412.